Electron Paramagnetic Resonance in Combination with the Thermal Analysis, X-ray Diffraction, and Raman Spectroscopy to Follow the Structural Properties of $Zr_xCe_{1-x}O_2$ Solid Systems and Precursors

Nicolas Sergent, Jean-François Lamonier, and Antoine Aboukaïs*

Laboratoire de Catalyse et Environnement, EA 2598, MREID, Université du Littoral-Côte d'Opale, 145, Av. Maurice Schumann, 59140 Dunkerque Cedex, France

Received April 14, 2000. Revised Manuscript Received September 26, 2000

The $Zr_xCe_{1-x}(OH)_4$ solids were prepared by simple precipitation of hydroxides from known solutions of $ZrOCl_2 \cdot 8H_2O$ and $Ce(NO_3)_3 \cdot 6H_2O$ in aqueous ammonium hydroxide. For $x \leq 0.5$, the presence of a CeO_2 phase with a mixed Zr−Ce hydroxide has been evidenced by thermal analysis and Raman and EPR spectroscopies. For this latter technique, the EPR signal of Ce^{3+} ions was used as a probe to determine the presence of the CeO_2 phase. For $x > 0.5$, a pure $Zr_xCe_{1-x}(OH)_4$ was found without the formation of the ZrO_2 phase. After calcination under flow air at 700 °C of hydroxide samples, $Zr_xCe_{1-x}O_2$ solid solutions were formed. For $x \leq 0.5$, the solids possess a cubic phase slightly modified from that corresponding to the pure CeO_2 phase structure, since the Zr^{4+} ions replace in the first step the Ce^{4+} ions located on the surface rather than in the bulk of CeO_2. For $x > 0.5$, the presence of Zr^{3+} ions corresponding to d^1 ions in an octahedral environment with strong tetragonal distortion was evidenced. This ion was used as a probe to determine the phase nature of the $Zr_xCe_{1-x}O_2$ solid solution. This phase was attributed to a tetragonal one except for the pure ZrO_2 solid, where a mixture of monoclinic and tetragonal phases was evidenced. As in the case of the XRD technique, EPR has been shown to efficiently evaluate the percentage of tetragonal or monoclinic phases in the ZrO_2 solid.

Introduction

Recently, a new generation of mixed oxides containing CeO_2 and ZrO_2 has been developed. Many studies have been reported concerning the preparation of zirconia−ceria solid solutions for application in various domains, in particular as component of three way catalysts for treatment of automotive exhaust gas. [1−2] The structure stability has been demonstrated for zirconia-doped ceria of cubic structure over a wide range of ceria concentration.[3] Depending on the Ce/Zr ratio and the calcination temperature, three different structures (monoclinic, tetragonal, or cubic) are observed by different techniques such as Raman spectroscopy, thermal analysis, and X-ray diffraction (XRD) for the ZrO_2−CeO_2 system.[1−7]

Despite the diversity of techniques used to elucidate the ZrO_2−CeO_2 systems, an ambiguity in the formation of solid solutions and their structures has been noticed, particularly those for which the Ce/Zr ratio is around 0.5. Colon et al.[8] have shown that for $Ce_{0.5}Zr_{0.5}O_2$ already calcined at 1200 °C, two new solid solutions with approximate compositions of 80% and 20% Ce were formed. Trovarelli et al.[9] have demonstrated that the utilization of mechanical milling for the preparation of catalysts based on CeO_2 structurally modified with ZrO_2 induces the formation of true solid solutions with a contraction of the cell parameter for cubic ceria following the introduction of Zr into the lattice. Hori et al.[10] have evidenced the formation of a ZrO_2−CeO_2 solid solution when this latter was prepared by precipitation of the corresponding hydroxides and calcination at 500 °C. In contrast, two separated phases (CeO_2 and ZrO_2) were formed when the preparation was performed by firing the corresponding acetate mixtures. The EPR technique, known for its high sensitivity, has been shown to be very powerful for following structural modifications of systems containing paramagnetic species. These latter can eventually exist in the systems or to be formed during thermal treatment.

The purpose of this work is to characterize mainly by EPR the structural modification of zirconium−cerium

* To whom correspondence should be addressed.

(1) Leitenburg, C.; Trovarelli, A.; Zamar, F.; Maschio, S.; Dolcetti, G.; Llorca, J. *J. Chem. Soc. Chem. Commun.* **1995**, 2181.
(2) Murota, T.; Hasegawa, T.; Aozasa, S.; Matsui, H.; Motoyama, M. *J. Alloys Compounds* **1993**, *193*, 298.
(3) Ozawa, M.; Kimura M.; Isogai, A. *J. Alloys Compounds* **1993**, *193*, 73.
(4) Fornasiero, P.; Balducci, G.; Di Monte, R.; Kaspar, J.; Sergo, V.; Gubitosa, G.; Ferrero, A.; Graziani, M. *J. Catal.* **1996**, *164*, 173.
(5) Moon, Y. T.; Park, H. K.; Kim, D. K.; Kim, C. H. *J. Am. Ceram. Soc.* **1995**, *78* (10), 2225.
(6) Fornasiero, P.; Di Monte, R.; Rango Rao, R.; Kaspar, J.; Meriani, S.; Trovarelli, A.; Graziani, M. *J. Catal.* **1995**, *151*, 168.
(7) Yashima, M.; Arashi, H.; Kakihana M.; Yoshimura, M. *J. Am. Ceram. Soc.* **1994**, *77* (4), 1067.
(8) Colon, G.; Pijolat, M.; Valdivieso, F.; Vidal, H.; Kaspar, J.; Finocchio, E.; Daturi, M.; Binet, C.; Lavalley, J. C.; Baker R. T.; Bernal, S. *J. Chem. Soc, Faraday Trans.* **1998**, *94*, 3717.
(9) Trovarelli, A.; Zamar, F.; Liorca, J.; de Leitenburg, C.; Dolcetti G.; Kiss, J. T. *J. Catal.* **1997**, *169*, 490.
(10) Hori, C. E.; Permana, H.; Simon Ng, K. Y.; Brenner, A.; More, K.; Rahmoeller K. M.; Belton, D. *Appl. Catal. B Environ.* **1998**, *16*, 105.

10.1021/cm000315d CCC: $19.00
Published on Web 11/22/2000

Table 1: Comparison of Experimental and Theoretical Mass Losses Obtained after the Calcination under Air of $Zr_xCe_{1-x}(OH)_4$ Samples

x ($Zr_xCe_{1-x}O_2$)	exptl mass loss	theor mass loss
0.00	7.1%	17.3%
0.25	8.2%	16.2%
0.50	12.4%	15.0%
0.75	11.2%	13.9%
0.80	12.9%	13.7%
0.85	12.9%	13.4%
0.90	11.9%	13.2%
1.00	13.6%	12.8%

systems obtained after precipitation and after calcinations under air flow at 700 °C.

Experimental Section

Different $Zr_xCe_{1-x}(OH)_4$ samples were prepared at room temperature by precipitation of hydroxides by addition of aqueous solutions of $ZrOCl_2 \cdot 8H_2O$ (0.15 M) and $Ce(NO_3)_3 \cdot 6H_2O$ (0.15 M) in desired quantities to aqueous ammonium hydroxide (0.7 M). This procedure enabled us to keep the pH > 9 and therefore to achieve simultaneous precipitation of the hydroxides. Thereafter, the hydroxide was carefully washed. To control and limit the presence of chloride in the zirconium-cerium hydroxides, the washing water was analyzed with an ionic chromatograph (Dionex DX 500). Therefore, after several washings with pure water, the concentration of chloride remaining in the hydroxide is less than 2 ppm. Finally, the solids were filtered and dried at 100 °C. The calcination treatment of the different hydroxides was carried out in a flow of dried air at 700 °C (60 °C h^{-1} heating rate and 4 h at calcination temperature). The calcined solid will be designated as $Zr_xCe_{1-x}O_2$.

The specific areas of samples are determined by the BET method using a Quantasorb Junior apparatus, and the gas adsorbed at −196 °C is pure nitrogen.

Thermal analysis measurements were performed with a Netzsch STA 409 equipped with a microbalance, differential thermal analysis (DTA), and a flow gas system. The dried zirconium-cerium hydroxides were treated under air (75 mL min^{-1}). The temperature was raised at a rate of 5 °C min^{-1} from room temperature to the desired temperature.

XRD data, for structural analysis, were collected at room temperature with a Siemens D5000 diffractometer using Cu Kα radiation (λ = 1.5418 Å) by placing the solids on quartz sample holders, at 2θ = 20−40° with a 0.02° step size. Background correction, $K\alpha_2$ stripping, and peak identification were accomplished with Diffract AT program (Siemens).

The Raman spectra were recorded with a Dilor XY monochromator with subtractive dispersion. The samples were excited using 632.8-nm radiation of a He−Ne laser.

The electron paramagnetic resonance (EPR) measurements are performed at 20 °C on a EMX Bruker spectrometer. A cavity operating with a frequency of 9.3 GHz (X-band) is used. The magnetic field is modulated at 100 kHz. Precise g values are determined from precise frequency and magnetic field values. All samples were subjected to various treatments before registration of EPR spectra. For each EPR measurement, a sample of about 0.4 g was used.

Results and Discussion

1. Untreated Solid: $Zr_xCe_{1-x}(OH)_4$. *1.1. Thermal Analysis.* Table 1 illustrates the weight loss of $Zr_xCe_{1-x}(OH)_4$ solids with calcination temperature. For the $Zr(OH)_4$ sample, the total loss of weight obtained after a calcination up to 700 °C was about 13.6%. This value indicates that this hydroxide is in the form of γ [$ZrO(OH)_2$] and not α [$Zr_4(OH)_{16}$] or/and β [$Zr_4O_2(OH)_{12}$].[11−13] The complete dehydration of the solid gave finally zirconia (ZrO_2). For the $Ce(OH)_4$ sample, the total loss of weight obtained up to 700 °C of calcination was about 7.1%. Since the theoretical value corresponding to a dehydration of $Ce(OH)_4$ to give CeO_2 solid is equal to 17.31%, it is then obvious to deduce that a large part of the hydroxide has been already transformed into CeO_2 during precipitation and drying of the solid at 100 °C.[14] When zirconium and cerium are present together ($Zr_xCe_{1-x}(OH)_4$), the total experimental weight loss increased when x passed from zero to 0.5. In the same range of x variation, when the weight losses are theoretically calculated from the hydroxide decomposition, a decrease of data was obtained. This difference can be explained by the diminution of the CeO_2 formation in the hydroxides. When x changed from 0.5 to 1, the total loss of weight remained constant and close to those calculated from the simple solid dehydration according to the formation, since precipitation, of a homogeneous $Zr_xCe_{1-x}(OH)_4$ solid without the formation of CeO_2.

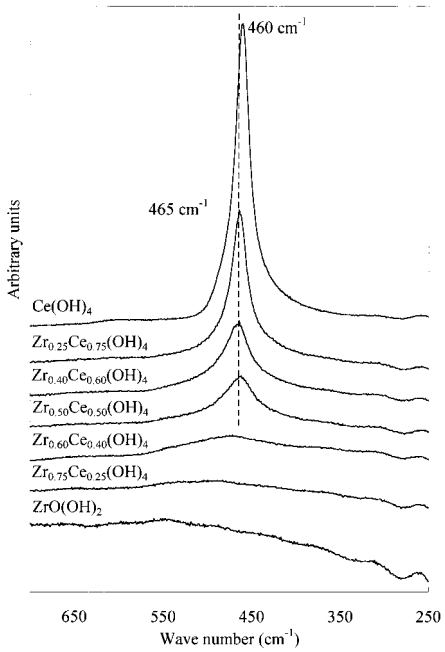

Figure 1. Raman spectra of $Zr_xCe_{1-x}(OH)_4$ samples in terms of x.

To confirm the presence or the absence of the CeO_2 phase since the precipitation of zirconium−cerium hydroxide, Raman and EPR spectroscopies were performed.

1.2. Raman Spectroscopy. Figure 1 illustrates the Raman spectra obtained in the 250−700 cm^{-1} range for different $Zr_xCe_{1-x}(OH)_4$ samples. The spectrum of pure cerium compound, $Ce(OH)_4$, exhibits a single band located at 460 cm^{-1}. This band is characteristic of the presence of a CeO_2 phase.[4] It is well-known that during the preparation of cerium hydroxide there is formation of a CeO_2 phase by partial dehydration of the precipitate.[14−15]

(11) Yamaguchi, T. *Catal. Today* **1994**, *20*, 199.

(12) Zaitsev, L. M. *Zh. Neorg. Khim.*, **1996**, *11*, 1684.

(13) Matta, J.; Lamonier, J. F.; Abi-Aad, E.; Zhilinskaya, E. A.; Aboukaïs, A. *Phys. Chem. Chem. Phys.* **1999**, *1*, 4975.

(14) Abi-Aad, E.; Bechara, R.; Grimblot J.; Aboukaïs, A. *Chem. Mater.* **1993**, *5*, 793.

(15) Kilbourn, B. T. *Cerium A Guide To Its Role In Chemical Technology*; Moly Corp, Inc.: White Plains, NY; 1992, p 14.

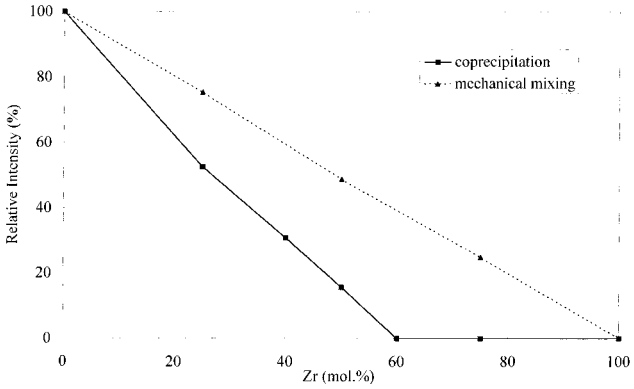

Figure 2. Evolution of the relative intensity of the 460 cm^{-1} Raman band in terms of zirconium content for $Zr_xCe_{1-x}(OH)_4$ and $xZrO(OH)_2 + (1 - x)Ce(OH)_4$ mixture samples.

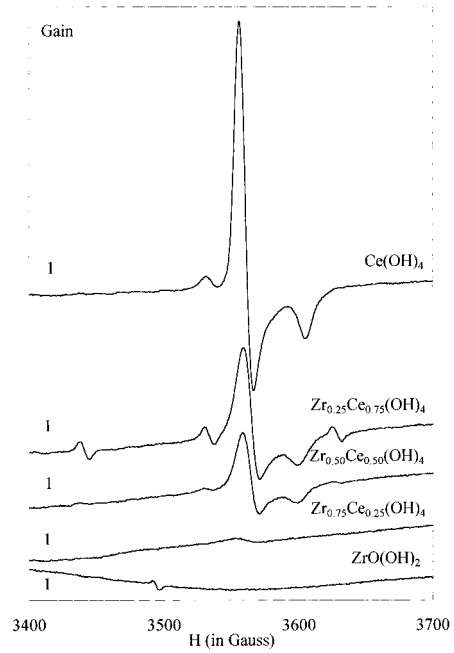

Figure 3. EPR spectra of $Zr_xCe_{1-x}(OH)_4$ samples in terms of x.

The intensity of this band is decreased by adding zirconium (Figure 2) and slightly shifted to higher wavenumbers (465 cm^{-1}). This shift can be related to a change in the CeO_2 environment in the presence of zirconium. Finally, the band disappeared when x > 0.5; this means that the CeO_2 phase is no longer present together with the $Zr_xCe_{1-x}(OH)_4$ solid. When the Raman band intensity of the latter hydroxide was compared to that obtained for a mechanical mixture of $ZrO(OH)_2$ and $Ce(OH)_4$ (Figure 2), it was always smaller for x ≤ 0.5. This result confirms that when both zirconium and cerium are simultaneously present one beside the other in a solid solution, the CeO_2 phase cannot be formed from the zirconium−cerium hydroxide. On the other hand, this phase will be formed from cerium hydroxide as is the case in the mechanical mixture. In addition, for $Zr_xCe_{1-x}(OH)_4$ where x > 0.5 and for pure $ZrO(OH)_2$, no trace of ZrO_2 phase was detected with the Raman technique.

1.3. EPR. Figure 3 shows the EPR spectra obtained for the untreated $Zr_xCe_{1-x}(OH)_4$ samples. A signal with axial symmetry ($g_\perp = 1.964$, $g_{||} = 1.938$, and $g_{iso} = 1.955$) was obtained for the $Ce(OH)_4$ sample. This signal, widely studied by numerous authors,[14,16−18] was attributed to the presence of Ce^{3+} ions in the CeO_2 matrix. The intensity of this signal decreased with an increase zirconium concentration in solids and finally disappeared for x > 0.5. The disappearance of the Ce^{3+} signal at such zirconium contents seems to be related to the absence of the CeO_2 phase. Indeed, it was demonstrated that the formation of the latter phase is due to a partial dehydration of the corresponding hydroxide precipitate where some OH^- groups can reduce the Ce^{4+} ions into Ce^{3+} before the formation of CeO_2 and H_2O.[15] The reduction of certain Ce^{4+} ions seems to occur when such ions are situated near other $Ce^{4+} - OH^-$ entities. In the presence of zirconium, the number of the latter species decreases and theoretically vanishes when $x = 0.5$. Consequently, during addition of the zirconium salt, the number of Zr−(OH)−Ce entities increases, whereas that corresponding to Ce−O−Ce decreases. This explains why the number of Ce^{3+} ions decreased and vanished for x > 0.5.

Table 2: Variation of Specific Areas of $Zr_xCe_{1-x}O_2$ Solids, Calcined at 700 °C, in Terms of x

x ($Zr_xCe_{1-x}O_2$)	specific area, m^2/g
0.00	41
0.25	36
0.50	61
0.75	58
0.80	46
0.85	43
0.90	44
1.00	38

From the thermal analysis and Raman and EPR spectroscopies results obtained on the untreated solid, it is evident that a pure $Zr_xCe_{1-x}(OH)_4$ phase is formed when the concentration of zirconium added to the solution is greater than that of cerium (x > 0.5). For x ≤ 0.5, the CeO_2 phase appeared in addition to the $Zr_xCe_{1-x}(OH)_4$ phase. This explains, first, the presence of a Ce^{3+} EPR signal and, second, the lower experimental weight loss values with respect to the theoretical ones obtained after the calcinations of untreated solids. For x > 0.5, the CeO_2 phase is absent as was demonstrated above by Raman spectroscopy and the formation of Ce^{3+} ions is not possible. This result explains why the theoretical and experimental weight losses obtained after calcination of the pure $Zr_xCe_{1-x}(OH)_4$ solid were similar. On the other hand, since with the Raman spectroscopy no trace of ZrO_2 was evidenced for $Zr_xCe_{1-x}(OH)_4$ samples, this can explain why no Zr^{3+} EPR signal has been observed for x > 0.5.

2. Solid Calcined at 700 °C: $Zr_xCe_{1-x}O_2$. *2.1. Specific Area.* Table 2 illustrates the specific areas obtained for different $Zr_xCe_{1-x}O_2$ samples (calcined at 700 °C under air). In the absence of zirconium (CeO_2), the specific area was 41 $m^2\ g^{-1}$, and it was 38 $m^2\ g^{-1}$ in the absence of cerium (ZrO_2). The specific area changed when zirconium and cerium are present together ($Zr_xCe_{1-x}O_2$), nevertheless, a maximum was obtained for $Zr_{0.5}Ce_{0.5}O_2$ sample (61 $m^2.g^{-1}$).

(16) Oliva, C.; Termignone, G.; Vatti, F. P.; Forni, L.; Vishniakov, A. V. *J. Mater. Sci.* **1996**, *31*, 6333.
(17) Aboukaïs, A.; Bennani, A.; Aïssi, C. F.; Wrobel G.; Guelton, M. *J. Chem. Soc., Faraday Trans.* **1992**, *88*, 1321.
(18) Fierro, J. L. G.; Soria, J.; Sanz, J.; Rojo, M. J. *J. Solid State Chem.* **1987**, *66*, 154.

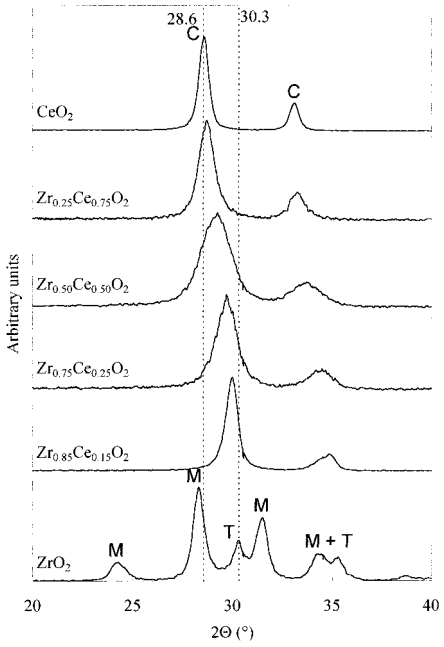

Figure 4. X-ray diffraction patterns of $Zr_xCe_{1-x}O_2$ solids, calcined at 700 °C, in terms of x.

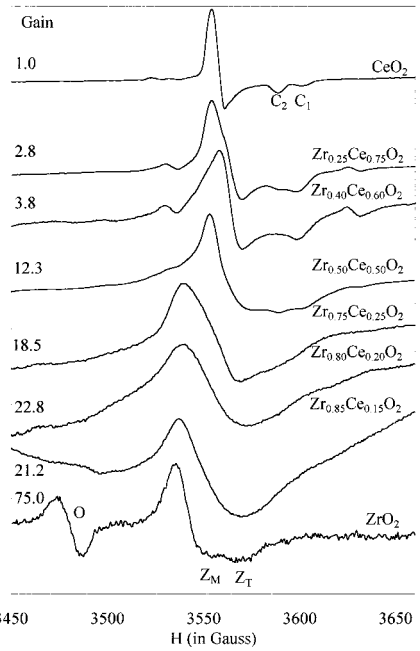

Figure 5. EPR spectra obtained for $Zr_xCe_{1-x}O_2$ solids, calcined at 700 °C, in terms of x.

2.2. X-ray Diffraction. Figure 4 illustrates the XRD patterns of $Zr_xCe_{1-x}O_2$ solids. Only the ceria cubic phase (CeO_2) was evidenced when the zirconium was absent in the solid.[10,17] Whereas for ZrO_2, a monoclinic phase (M) was formed with a small amount of tetragonal phase (T). The relative amount of the tetragonal phase (x_T) was calculated from an equation already used elsewhere:[13]

$$x_T = \frac{I_T(111)}{I_M(111) + I_M(11\bar{1}) + I_T(111)}$$

where I_T and I_M are the integrated intensities of the tetragonal and monoclinic phases, respectively. For the calculation of intensities, a new profile program of Diffract AT (Siemens) was used and a ratio of 0.68 for $I_M(11\bar{1})/I_M(111)$ and the position of monoclinic and tetragonal lines were imposed. The x_T value was found to be equal to 0.19.

The XRD lines obtained in the case of CeO_2 are totally different from those obtained for the ZrO_2 solid. On the other hand, for solids containing simultaneously zirconium and cerium ($Zr_xCe_{1-x}O_2$), the XRD lines are rather similar to those corresponding to the CeO_2 phase and not to the ZrO_2 phase, even for high zirconium content. Indeed, when the zirconium concentration increased with respect to that of cerium, a shift of CeO_2 phase lines toward higher values of 2θ was observed. This phenomenon, which has been observed by numerous authors,[8,10,19,20] can be explained by the insertion of zirconium atoms in the CeO_2 cubic matrix with the contraction of its cell parameter and the deformation of the cubic phase to be transformed into the tetragonal phase for higher zirconium contents. Indeed, it is well-known that the CeO_2 solid has the fluorite structure, space group $Fm3m$, with 8-coordinate cations and 4-coordinate anions, for which the ionic radius ratio of Ce^{4+} to O^{2-} (R_{Ce4+}/R_{O2-}) is equal to 0.782, whereas, in the perfect fluorite structure, this latter ratio must correspond to 0.732. Since the ionic radius of Zr^{4+} (0.82 Å) is smaller than that of Ce^{4+} (0.97 Å), consequently, the partial insertion of zirconium in CeO_2 can decrease the ionic radius ratio and leads to stabilization of the fluorite structure when this ratio reaches 0.732. Since in the pure ZrO_2, the $R_{Zr^{4+}}/R_{O^{2-}}$ ratio is equal to 0.66, the theoretical substitution of 50% of cerium by zirconium in CeO_2 can give a $(R_{Zr^{4+}} + R_{Ce^{4+}})/R_{O^{2-}}$ ratio of 0.73 and a stable $Zr_{0.5}Ce_{0.5}O_2$ solid solution.

In addition, compared to CeO_2 XRD lines, the $Zr_xCe_{1-x}O_2$ lines are broader. The widths of lines increased with the zirconium content to reach a maximum for the $Zr_{0.5}Ce_{0.5}O_2$ sample and subsequently decreased. Since the line widths are related to the size of particles, $x = 0.5$ corresponds to the smallest particles of these solid series. These results are in qualitative agreement with specific area data, where a maximum is obtained (61 $m^2\ g^{-1}$) for the $Zr_{0.5}Ce_{0.5}O_2$ sample.

2.3. EPR. Figure 5 shows the EPR spectra recorded at 20 °C for $Zr_xCe_{1-x}O_2$ solids. The spectrum obtained in pure CeO_2 has been widely studied elsewhere.[14,16−18] In fact, this spectrum is composed of two signals denoted by C_1 and C_2 and apparently characterized by $g_{1\perp} \sim g_{2\perp} \sim 1.965$, $g_{1||} = 1.940$, and $g_{2||} = 1.946$. These signals can be attributed to the presence of Ce^{3+} ions located at two different sites.[14,17] Indeed, when zirconium is introduced into the CeO_2 matrix, the intensity of the C_2 signal decreased and vanished for $Zr_{0.40}Ce_{0.60}O_2$, whereas the C_1 signal intensity remained stable with $g_{1\perp} = 1.963$ and $g_{1||} = 1.941$. Consequently, the C_2 signal admits as g values $g_{2\perp} = 1.965$ and $g_{2||} = 1.946$. Since the C_2 signal disappeared after introduction of zirconium into CeO_2, it is suggested that the Ce^{3+} ions corresponding to that signal can be located on the CeO_2 surface, whereas those corresponding to the C_1 signal are in the CeO_2 bulk. This

(19) Yao, M. H.; Baird, R. J.; Kunz, F. W.; Hoost, T. E. *J. Catal.* **1997**, *166*, 67.
(20) Fornasiero, P.; Fonda, E.; Di Monte, R.; Vlaic, G.; Kaspar, J.; Graziani, M. *J. Catal.* **1999**, *187*, 177.

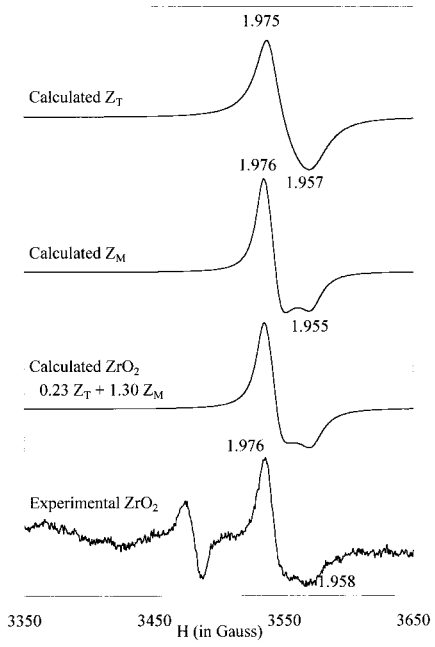

Figure 6. Calculated Z_T and Z_M signals and their summation with respect to relative intensities to give a calculated ZrO_2 spectrum.

hypothesis can be confirmed by the fact that in the case of untreated solids, $Zr_xCe_{1-x}(OH)_4$, the EPR signal obtained is similar to the C_1 and not the C_2 signal. Since the OH groups in the $Zr_xCe_{1-x}(OH)_4$ phase are located on the solid surface rather than in the bulk. Consequently, the CeO_2 phase which is present in these solids must be located in the bulk. And since the CeO_2 phase is the precursor of Ce^{3+} ions, these latter species are located in the solid bulk. In conclusion, for small amounts of zirconium, the Zr^{4+} ions replace in the first step the Ce^{4+} ions located on the surface rather than in the bulk of CeO_2.

The spectrum obtained for pure ZrO_2 is apparently composed of three signals denoted by Z_M, Z_T, and O (Figure 5). When cerium is introduced in small amounts with respect to zirconium ($Zr_{0.85}Ce_{0.15}O_2$), the intensities of Z_M and O signals drastically decreased and finally vanished for $Zr_{0.80}Ce_{0.20}O$, whereas that of Z_T is slightly increased. When the concentration of cerium is increased to $Zr_{0.75}Ce_{0.25}O_2$, the intensity of this latter signal is further decreased and becomes negligible for $Zr_{0.50}Ce_{0.50}O_2$, whereas two signals (C_1 and C_2) with weak intensities become detectable and can be attributed to Ce^{3+} traces located in small amounts of CeO_2 remaining in the $Zr_xCe_{1-x}O_2$ solid solution as impurities.

The Z_T signal is apparently symmetric and centered at $g = 1.966$ with peak-to-peak width $\Delta H = 32.7$ G. From these latter data, the EPR parameter values of Z_M and Z_T signals in ZrO_2 solid and their relative intensities were precisely determined after comparison of the experimental with the calculated signals (Figure 6 and Table 3). The g signal values are in agreement with the expected ones for a d^1 ion in an octahedral environment with strong tetragonal distortion.[13,21−24] The Z_M and Z_T signals were attributed respectively to Zr^{3+} ions located in monoclinic and tetragonal phases. Indeed, for the ZrO_2 solid, the monoclinic and tetragonal phases were evidenced with the XRD technique, whereas

Table 3: EPR Parameters Values of $Zr_xCe_{1-x}O_2$ Solids, Calcined at 700 °C, in Terms of x

	Zr^{3+}				Ce^{3+}			
sample	$g_\perp Z_M$	$g_\parallel Z_M$	$g_\perp Z_T$	$g_\parallel Z_T$	$g_\perp C_1$	$g_\parallel C_1$	$g_\perp C_2$	$g_\parallel C_2$
CeO_2					1.965	1.940	1.965	1.946
$Zr_{0.25}Ce_{0.75}O_2$					1.965	1.941	1.965	1.945
$Zr_{0.40}Ce_{0.60}O_2$					1.963	1.941		
$Zr_{0.50}Ce_{0.50}O_2$			1.972	1.953	1.966	1.940		
$Zr_{0.75}Ce_{0.25}O_2$			1.973	1.957		1.950		
$Zr_{0.80}Ce_{0.20}O_2$			1.973	1.955				
$Zr_{0.85}Ce_{0.15}O_2$			1.975	1.957				
ZrO_2	1.976	1.965	1.976	1.958				

for $Zr_{0.85}Ce_{0.15}O_2$, $Zr_{0.80}Ce_{0.20}O_2$, and $Zr_{0.75}Ce_{0.25}O_2$ solids, Raman spectroscopy has shown the presence of the tetragonal phase only. This result is in a good agreement with the absence of the Z_M signal for the latter solids. The percentage value of tetragonal phase calculated by EPR simulation was 16%. This result was in good agreement with those above obtained (19%) with the XRD technique. The formation of Zr^{3+} species in $Zr_xCe_{1-x}O_2$ solids is probably due to the dehydration of the zirconium hydroxide, where some OH^- groups can reduce the Zr^{4+} ions before the formation of ZrO_2 and H_2O. Indeed, Chen et al.[22] have suggested that the formation of Zr^{3+} ions in the sulfated zirconia is due to the reduction by SO_4^{2-} of the Zr^{4+} to Zr^{3+} species.

The O signal observed in ZrO_2 with the Z_M and Z_T signals has an axial symmetry with $g_\parallel = 2.020$ and $g_\perp = 2.005$. Similar signals have been already obtained elsewhere[14,25−26] and have been attributed to O_2^- species adsorbed on the solid matrix. This signal disappeared with the Z_M signal when a small amount of cerium is present with zirconium ($Zr_{0.85}Ce_{0.15}O_2$). This disappearance can be related to the oxidation of Zr^{3+} ions (Z_M) with the oxygen species to give Zr^{4+} ions.

Conclusion

This work studies the $Zr_xCe_{1-x}(OH)_4$ and $Zr_xCe_{1-x}O_2$ solids after their preparation by simple precipitation and calcination under air at 700 °C. For this purpose, mainly the EPR technique in combination with thermal analysis, Raman, and XRD ones have been used.

It was demonstrated that Ce^{3+} and Zr^{3+} ions could be used as ion probes in the solids. The first one was related to the cubic CeO_2 phase presence while the second to the monoclinic or/and tetragonal $Zr_xCe_{1-x}O_2$ solids.

By precipitation of $Zr_xCe_{1-x}(OH)_4$ hydroxides from known solutions of $ZrOCl_2 \cdot 8H_2O$ and $Ce(NO_3)_3 \cdot 6H_2O$ in an aqueous ammonium hydroxide, a CeO_2 phase is evidenced for $x \leq 0.5$. For $Zr_xCe_{1-x}O_2$ solids, the phase is cubic when $x = 0$ since it corresponds to the CeO_2

(21) Torralvo, M. J.; Alario M. A.; Soria, J. *J. Catal.* **1984**, *86*, 473. Morterra, C.; Giamello, E.; Orio, E.; Volante, M. *J. Phys. Chem.* **1990**, *94*, 3111.
(22) Chen, F. R.; Coudurier, G.; Joly, J. F.; Vedrine, J. C. *J. Catal.* **1993**, *143*, 616.
(23) Bobricheva, I. V.; Stavitsky, I. A.; Yermolaev, V. K.; Kotsarenko, N. S.; Shmachkova V. P.; Kochubey, D. I. *Catal. Lett.* **1998**, *56*, 23.
(24) Markaryan, G. L.; Ikryannikova, L. N.; Muravieva, G. P.; Turakulova, A. O.; Kostyuk, B. G.; Lunina, E. V.; Lunin, V. V.; Zhilinskaya, E.; Aboukaïs, A. *J. Colloids Surf. A: Physicochem. Eng. Aspects* **1999**, *147*, 435.
(25) Che, M.; Tench, A. *J. Adv. Catal.* **1983**, *32*, 1.
(26) Zhang, X.; Klabunde, K. *J. Inorg. Chem.* **1992**, *31*, 1706.

solid. This phase remained stable with slight modification, while $x \leq 0.5$. On the other hand, for $x > 0.5$, the cubic phase of $Zr_xCe_{1-x}O_2$ transforms into a tetragonal phase, and for $x = 1$, a monoclinic phase is detected with the tetragonal one.

Acknowledgment. We thank the Conseil Général du Nord, the Région Nord-Pas de Calais, and the European Community (European Regional Development Fund) for financial supports in the EPR and thermal analysis apparatus purchase. We also thank INTAS for grants under which this work was carried out. Moreover, we thank Mrs. Zhilinskaya for her EPR contribution.

CM000315D